Size-selective filtration of the atrial wall estimated from the accumulation of tracers in the kidney of the mussel *Mytilus galloprovincialis*

Authors:

Hidefumi Wakashin[1]*, Eriko Seo[2]* and Yoshiteru Seo[1,]**

Affiliations:

1. Department of Regulatory Physiology, Dokkyo Medical University School of Medicine, Tochigi, 321-0293, Japan
2. Department of Marine Ecosystem Dynamics, Division of Marine Life Science, Atmosphere and Ocean Research Institute, The University of Tokyo, Kashiwa, 277-8564, Japan

*: Authors who contributed equally

**: Corresponding author

E-mail address: yseo@dokkyomed.ac.jp

Keywords:

Nephridia, Glomerular filtration, T_1 relaxation time, Magnetic resonance imaging

Summary statement:

Magnetic resonance imaging showed accumulation of the injected tracers in the kidney. The atrial wall of the *Mytilus galloprovincialis* could filtrate small molecules (< 0.5 kDa), but not larger molecules.

ABSTRACT

In order to determine the molecular weight cut-off (MWCO) for the atrial wall filtration into kidneys of the *Mytilus galloprovincialis*, we employed 5 magnetic resonance (MR) tracers: manganese chloride (Mn^{2+}), gadolinium chloride (Gd^{3+}), manganese-ethylenediaminetetraacetic acid (MnEDTA), gadolinium-diethylenetriamine pentaacetic acid (GdDTPA), and oligomer-based contrast agent (CH3-DTPA-Gd). After injection of the MR tracers (1 or 2 mM x 0.1 mL) into the visceral mass, T_1-weighted MR imaging (T_{1w}-MRI) and the longitudinal relaxation rates ($1/T_1 = R_1$) were measured at 20°C. The MR tracers were distributed uniformly in the visceral mass within 1 h after injection. The T_{1w}-MRI intensity and R_1 of the kidney (R_{1K}) were increased by Mn^{2+} and MnEDTA, with urine concentrations estimated at 210 and 65 μM, respectively. The rest of tracers showed only minimal or no increase. When the mussels were additionally incubated in seawater with 10 μM $MnCl_2$, R_{1K} was increased in the GdDTPA group, but not in the $GdCl_3$ group. Therefore, Gd^{3+} might have inhibited renal accumulation of Mn^{2+} and Gd^{3+}. Incubation in seawater with 10 μM MnEDTA showed no increase in the R_{1K}, but additional incubation with 10 μM $MnCl_2$ caused an increase in R_{1K}. It is suggested that injected MnEDTA was filtrated as MnEDTA per se, and not likely separated into free Mn^{2+}. Thus, we concluded that the MWCO of the atrial wall of the *Mytilus galloprovincialis* is around 0.5 kDa, which is almost 1/100 of that for vertebrate animals, and suggests a reduction in efforts to reabsorb metabolites and osmolytes from the urine.

INTRODUCTION

The excretion system of mussels consists of kidneys and the pericardium (Martin and Harrison, 1966; Bayne, 1976) As shown in a diagram in Fig. 1, hemolymph is filtered into the pericardial cavity by the atrial wall or the pericardial gland in the heart. Then, the filtrate flows to the nephridia sac (kidney), and secretion, absorption and storage might be attributed to the kidneys (Martin and Harrison, 1966; Bayne, 1976). Morphological evidence of filtration was obtained by an electron microscopic study on the atrial wall of the *Mytilus* heart (Pirie and Geoge, 1979; Andrews and Jennings, 1993). Physiological studies of bivalves were initially conducted by Picken (1937). Body fluid directly collected from the pericardial cavity of *Anodonta cygna* by needle was approximately isotonic (Picken, 1937). According to the constant-volume hypothesis (Ramsay, 1952; Krijgsman and Divaris, 1955; Seo et al., 2014a), it was expected that there would be filtration pressure, and this was confirmed by the atrial and pericardial pressure in *Anodonta anatine* (Brand, 1972) and also by the flow direction in the renopericardial canal of the *Mytilus galloprovincialis* (Seo et al., 2014a). Therefore, it can be considered that filtration occurs via the atrial wall.

The characteristics of the filtration wall of bivalves have not been well analyzed to the present date. As far as we found in a search of investigative reports, the excretion system of the abalone, *Haliotis rufescens*, could filtrate *p*-amino hippuric acid (PAH, 0.19 kDa), phenolsuphonphthalein (PSP, 0.35 kDa) and inulin (5.5 kDa) (Harrison, 1962). Filtration of inulin was also reported in the octopus and the African snail (Martin and Harrison, 1966). Inulin is the common substance for measurement of the glomerular filtration rate in the vertebrate (Guyton and Hall, 2006). However, the evidence available is not convincing in regard to whether or not the atrial wall of the *Mytilus* filtrates inulin, due to the following reasons: amino acids, such as taurine and betaine, are important osmolytes for the hemolymph in the *Mytilus edulis* (Bayne, 1976), and the cell release/uptake of osmolytes varies when seawater shows lower or higher salinity (Burton, 1983; Hoyaux et al., 1976). If the mussel filters out large substances such as inulin (5 kDa), 1) the mussel may lose a lot of metabolites and osmolytes from the hemolymph, and 2) the kidney has to reabsorb a lot of metabolites and osmolytes from the urine. However, the structure of the canal between the pericardial

cavity and the nephridia is different from the tubular formation seen in the vertebral kidney, being comparably short and not convoluted. It is not clear whether the canal actively reabsorbs osmolyte to maintain osmolarity of body fluid. Considering that the nephridia or kidney of the mussel has a luminal structure which is drained by the auricle filtrates via the canal, the physiological function of the atrial barrier for the substrate should be different from that seen in the vertebrate. Therefore, we were motivated to determine the molecular size barrier of the atrial wall. In human renal tubules, small molecules, such as glucose and oligopeptides (up to 4 amino acids) are transported by the specific transporters. Larger molecules such as polypeptides and immunoglobulins are reabsorbed by endocytosis, which is slower than the oligopeptides transport, and much more energy is required in the process for the kidney epithelia (Boron and Boulpaep, 2004). Therefore, we assumed the hypothesis that the auricle wall could not filter molecules larger than 0.5 kDa.

In order to test this hypothesis, magnetic resonance (MR) tracers were employed with varying molecular weights from 0.05 to 2 kDa. In our previous report, a magnetic resonance imaging (MRI) method was applied to observe heavy metal ion (Mn^{2+}) accumulation in the kidney of the *Mytilus galloprovincialis* (Wakashin et al., 2018). MR tracers are paramagnetic, and accelerate the longitudinal relaxation rate ($1/T_1 = R_1$). Thus, when MR tracers are injected in the hemolymph of the visceral mass, the R_1 is increased, depending on the concentration as follows: $R_1 = R_0 + K \cdot C$, where R_0, K and C are the intrinsic R_1 of the hemolymph, the relaxivity value of the MR tracer ($mM^{-1}\ s^{-1}$), and the concentration of the MR tracer (mM), respectively. Therefore, R_1 in the kidney should be increased when MR tracers are filtrated in the atrial wall, and concentrated in the kidney (Fig. 1). T_{1w}-MRI intensity ($M(R_1)$) with a short echo-time could be written as follows:

$$M(R_1) = M_O \bullet \sin\theta \bullet [1 - \exp(-T_R \cdot R_1)] / [1 - \cos\theta \bullet \exp(-T_R \cdot R_1)],$$

where M_O is the equilibrium image intensity, and T_R and θ are the repetition time and the flip angle of the excitation pulse, respectively. Thus, an increase in the R_1 could be detected as a higher signal intensity in T_1-weighted MRI (T_{1w}-MRI). Five kinds of magnetic resonance (MR) tracers were employed as follows: 1) Oligomer-based contrast agent (CH3-DTPA-Gd; 2.1 kDa) is developed as an intravascular contrast agent due to its large molecular size. 2)

gadolinium-diethylenetriamine pentaacetic acid (GdDTPA; 0.55 kDa) is the most popular MR tracer in clinical medicine, and it is used as an extracellular contrast agent. 3) manganese-ethylenediaminetetraacetic acid (MnEDTA; 0.35 kDa) is also extracellular contrast agent. 4) manganese ion (Mn^{2+}; 0.055 kDa) is used to detect brain functional MR imaging (Lin & Koretsky, 1997). Since Mn^{2+} has a close chemical similarity with Ca^{2+}, Mn^{2+} inhibits the L-type Ca^{2+} channel (Yang, 2006), and have to keep Mn^{2+} concentration lower than 100 μM (Seo et al., 2013). 5) Gadolinium ion (Gd^{3+}; 0.16 kDa) has a high toxicity to block Ca^{2+}-dependent processes in various cells, including muscles, neurons and epithelial cells at 2-3 μM (Rogosnitzky and Branch, 2016). In this study, Gd^{3+} was used not only as an MR tracer but also as an inhibitor of Ca^{2+} (Mn^{2+}) transport systems. Using these MR tracers, 1) we measured T_{1w}-MRI and R_1 of the urine in the kidney of mussels enhanced by MR tracers, and 2) evaluated the relationship between the molecular weight of 4 MR tracers and the R_1 of the urine in the kidney. We also examined the 3) toxicity and stability of the MR tracers using Gd^{3+}. Judging from these results, we were able to determine the molecular weight cut-off (MWCO) for filtration by the atrial wall in the heart of the mussel, *Mytilus galloprovincialis*.

MATERIALS AND METHODS

Experimental mussels

The *Mytilus galloprovincialis* Lamarck 1819 used in this study were collected from a subtidal zone of the shore of Hisanohama, Fukushima in February 27, 2019. At the laboratory, in 3 separate 5 L baths, 15-20 mussels were kept in each bath in aerated synthetic seawater (salinity 36‰) at room temperature (20-24°C) (Seo et al., 2014b). Salinity of the seawater was measured by a refractometer (Master-S28α, Atago, Tokyo, Japan), and half of the seawater was replaced every week. A total of 47 mussels were used in this MRI study. The length, height and width of the mussels was 35.7 ± 0.4 mm, 19.4 ± 0.2 mm and 14.1 ± 0.2 mm (mean and s.e.m), respectively. All of the animal experiments in this study were carried out under the rules and regulations of the "Guiding Principles for the Care and Use of Animals" set by the Physiological Society of Japan, and approved by the Animal Research Councils at Dokkyo University School of Medicine.

MR tracers and measurement of relaxivity

Five kinds of MR tracers were used for the tracer study as follows: Mn^{2+} as manganese chloride (nacali, Kyoto, Japan), Gd^{3+} as gadolinium chloride (Wako, Osaka, Japan), MnEDTA was made from $MnCl_2$ and Na_2EDTA (DOJINDO, Kumamoto, Japan), GdDTPA (Magnevist, Schering, Berlin, Germany), CH3-DTPA-Gd (NMS-60, Nihon Medi-Physics, Chiba, Japan). These tracers were dissolved in 36‰ NaCl solution, and the R_1 values of the solutions (0 – 1 mM) were measured by inversion recovery pulse sequences with a 20-mm ^{1}H coil at 20°C. The relaxivity of the tracers were calculated from the slope of a linear regression line by using Excel 2016 (Microsoft, Redmond, WA, USA).

Magnetic resonance imaging

The MRI examination of the *M. galloprovincialis* in this study used procedures noted in our previous reports (Seo et al., 2014a; 2016, Wakashin et al. 2018). In brief, the mussels were placed in a plastic tube (inner diameter of 22.5 mm), and were immersed in 12 mL of synthetic seawater without aeration, and the temperature was kept at 20°C. Seawater was exchangeable through another tube set in the bottom of the tube holding the mussel. The ^{1}H MR images were obtained by a 7 T vertical magnetic resonance imaging system (AVANCE III, Bruker Biospin, Ettlingen, Baden-Württemberg, Germany) with ParaVision operating software (version 5.1) and equipped with an active shielded gradient (micro2.5) and a 25-mm ^{1}H birdcage radiofrequency coil.

R_1 relaxation rate was measured by a two-dimensional saturation-recovery imaging method with 5 relaxation delays from 0.1 sec to 4 sec. The pixel size was 180 x 180 μm and the slice thickness was 1 mm. The total image acquisition time was 9 min 21 s. The R_1 image was calculated by Image Sequence Analysis Tool of ParaVision. Images with a large motion artifacts were omitted from the following data analysis. In order to include the whole-body structure of the mussel, three-dimensional T_1-weighted gradient-echo imaging (3D T_{1w}-MRI) was used. The MR signal in the kidney was analysed by 3D T_{1w}-MRI with a voxel size of 240 × 240 × 240 μm, and a combination of $T_R/T_E/\theta$ = 50 ms/2.5 ms/22.5º, where T_R, T_E and θ are

relaxation delay, echo-time and flip angle, respectively. The total image acquisition time was 7 min 40 s. Images were Fourier-transformed with a data matrix of 256 × 128 × 128 after zero-filling of data, and the final voxel size was 180 × 180 × 180 μm. The volume of the kidney was obtained by using a 3D-MRI analysis package of ParaVison. The image intensity of the T_{1w}-MR image was quantified compared with the image intensity of reference capillary containing 0.5 mM $MnCl_2$ solution. Statistical analysis of R_1 was applied by unpaired or paired *t*-test using Excel 2016 (Microsoft, Redmond, WA, USA). *P* values less than 0.05 were regarded as significant.

Injection of MR tracers

Mussels were anesthetized by 4 % $MgCl_2$, 0.1 mL 36‰ NaCl solution containing 1 or 2 mM MR tracers were injected into the visceral mass near the root of the foot by a 30G needle (Nipro, Osaka, Japan). Injection of the MR tracers was confirmed by noting a higher signal intensity of the visceral mass in scout T_{1w}-MR images.

Protocols of MR experiments

The protocols of the 3 types of MR experiments are summarized in Fig. 2. Experiments on the accumulation of the MR tracers in the kidney (Fig. 2A) started from the injection of the MR tracers. Then, the mussels were incubated in the control seawater. The R_1 relaxation rate was measured at 1, 2 and 3 h after the injection, and 3D T_{1w}-MR images were measured between the R_1 measurements. When the atrial wall could filter the MR tracer, the T_{1w}-MRI intensity and the R_1 of the kidneys increased, and *vice versa* (Fig.1).

Experiments on the effects of GdDTPA or Gd^{3+} on the renal function (Fig. 2B) also started from the injection of GdDTPA or Gd^{3+}, followed by 3 or 1 set of measurements of the 3D T_{1w}-MR image and the R_1 relaxation rate, respectively. Then, the seawater was replaced by seawater containing 10 μM $MnCl_2$, and 3D T_{1w}-MR images and R_1 relaxation rates were observed at 1 h after incubation. If GdDTPA or Gd^{3+} inhibited the renal function, we could not detect any increase in the T_{1w}-MRI intensity or R_1 even with the additional incubation in seawater containing Mn^{2+} (Fig.1).

The experiments on the stability of the MnEDTA and the toxicity of Gd^{3+} (Fig. 2C) were started from the incubation of the mussels in seawater containing 10 μM of MnEDTA or $GdCl_3$ for 1 h. Then, seawater was replaced by seawater containing 10 μM of $MnCl_2$. The R_1 relaxation rate was measured before and 1 h after the Mn^{2+} incubation. If the Gd^{3+} inhibited Mn^{2+} uptake from the seawater (supposed by digestive and/or gill epithelia) (Fig. 1), we could not detect any increase in the T_{1w}-MRI intensity or R_1 with the additional incubation in the seawater containing Mn^{2+}. When the MnEDTA released free Mn^{2+} in the seawater, we could detect an increase in the T_{1w}-MRI intensity and R_1.

In order to minimize the length of the MR experiments, the R_1 for the control condition was taken as the mean R_1 value obtained in separate experiments.

RESULTS

Relaxivity of MR tracers

First, we examined the concentration dependency of the MR tracers on the R_1 relaxation rate. The results are shown in Fig. 3. As mentioned in the Introduction, the R_1 value depends on the concentration of the MR tracer, the relaxivity values calculated from the slope of the linear regression line are shown in the table underneath Fig. 3.

Distribution and accumulation of the MR tracers in the kidney

The injection of the MR tracers was confirmed using scout T_{1w}-MR images. When MR tracers were injected into the visceral mass near the root of the foot, the T_{1w}-MR image intensity of the visceral increased due to the increase in R_1 caused by the MR tracers. Therefore, the image intensity of the foot was depicted as a higher signal intensity at 10 min after the injection of GdDTPA (Fig. 4A, B). Then, the image intensity of the foot decreased, dependent on the time course (Fig. 4C). Usually, the image intensity reached an almost uniform intensity until 1 h after the injection (Fig. 4D). As shown in Fig. 4D, the T_{1w}-MR image intensity of the visceral mass and also the mantle were almost the same degree, representing uniform distribution of GdDTPA in the hemolymph of the mussel. As shown in

Fig. 4H, in a few cases, the MR tracers remained at a high concentration in the tip of foot, suggesting that the dynamics of the tracers could be affected by a local factor.

In order to indicate the position of the kidneys, pairs of longitudinal slices at the kidney and a transverse slice at 2 mm posterior to the atrioventricular valve of a mussel fixed in paraformaldehyde are shown in Fig. 4E (Wakashin et al., 2018). When Mn^{2+} injected in the mussel, only the lumen inside of the kidneys showed a higher intensity, which represents the accumulation of Mn^{2+} in the urine (Fig. 4F). Similar results were also obtained after the injection of MnEDTA (Fig. 4G). The mean and s.e.m. of the volume of kidney was 9.2 ± 0.49 μL (n = 23), as estimated from a 3D reconstructed image of the kidney.

The GdDTPA and CH3-DTPA-Gd were also distributed equally in the interstitial space (Fig. 4H, I). However, the T_{1w}-MR image intensity of the kidney was not enhanced, and remained at almost the same intensity as that of the seawater. These low intensity regions could be enhanced by additional incubation with 10 μM $MnCl_2$ (Fig. 4J). Therefore, we confirmed that these regions were kidneys, and that GdDTPA and CH3-DTPA-Gd are not accumulated in the urine. The injected Gd^{3+} showed a different distribution, compared with that of the GdDTPA pattern (Fig. 4K). The T_{1w}-MR image intensity of the borders of the kidney, intestine, stomach and gills were enhanced. Urine in the kidney was not enhanced, even after 1 h of additional incubation with 10 μM $MnCl_2$.

Changes in the R_1 relaxation rate of the kidney and foot.

We also examined time dependent changes of R_1 in the mussel, and the results were summarized at 1, 2 and 3 h after the injection of the MR tracers (Fig. 5). The proximal side of the foot (Fig. 4E) was used for the typical point of the tracing in the visceral mass. In the kidney, the injection of $MnCl_2$ and MnEDTA caused an increase in R_1, compared with the control (P <0.01), which remained at the same level for 3 h (P >0.05). The injection of CH3-DTPA-Gd and GdDTPA showed no or a minimal increase in R_1 for 3 h, compared with the control (P >0.05). In the foot, R_1 increased significantly after the injection of $MnCl_2$ and CH3-DTPA-Gd (P <0.01 or 0.05).

The means and s.e.m. of R_1 at 1 h after the injection of the MR tracers are summarized in Fig. 6A. The concentrations of the MR tracers were estimated by $C = (R_1 - R_c) / K$, where R_c and K are the R_1 of the control and the relaxivity value of the MR tracers. As shown in Fig. 6B, the kidney concentration of Mn^{2+} and MnEDTA were higher than the foot (P <0.01), and were estimated as 213 ± 22 and 65 ± 8 μM (mean ± s.e.m., n=14), respectively. There were no differences between the concentration of GdDTPA in the kidney and the foot (P >0.05). The concentrations of CH3-DTPA-Gd and Gd^{3+} in the kidney were lower than that in the foot (P <0.01). Therefore, GdDTPA, CH3-DTPA-Gd and Gd^{3+} were not concentrated in the kidney, even though the interstitial concentration of the MR tracers was around 50 μM.

The dose dependency of the CH3-DTPA-Gd injection was shown in Fig. 7. There was a linear relationship with a slope of 0.236 ± 0.032 $(s \cdot mM)^{-1}$ (coefficient ± s.e.m.). The slope was 1/20 of the relaxivity of the CH3-DTPA-Gd (4.8 $(s \cdot mM)^{-1}$). Therefore the injected tracers (0.1 mL) were diluted 20 fold in the mussel. Since CH3-DTPA-Gd could not enter cells and was not filtered into the urine, the total volume of the hemolymph could be estimated as 2.0 (1.6 – 2.8) mL (95% confidence limits).

Effects of the MR tracers on renal function.

In order to check the effect of the interstitial MR tracers (50 μM) on the function of the kidney, seawater was replaced by fresh seawater containing 10 μM of $MnCl_2$ at 3 h after the injection of the GdDTPA. As shown in Fig. 8A, the R_1 of the kidney did not increase with the injection of 1 mM GdDTPA as expected, but it was increased by the additional incubation with Mn^{2+} (P <0.05). Therefore, GdDTPA does not affect the accumulation of Mn^{2+}. On the contrary, when 1 mM $GdCl_3$ was injected, no elevation of the renal R_1 was observed, and importantly, the expected enhancement of renal R_1 due to the additional incubation with Mn^{2+} (P >0.05) was not reproduced. In addition, as shown in Fig. 8B, the R_1 of the kidney was not increased by incubation in seawater containing 10 μM of $GdCl_3$, nor was it increased by the additional incubation in 10 μM of Mn^{2+} (P >0.05). These data indicated that Gd^{3+} functionally inhibited Mn^{2+} uptake from seawater and the concentration in the kidney (Fig. 1).

The stability constant of the metal complex is represented by pK_M = log ([ML] /[M] [L]), where [ML], [M] and [L] are the concentrations of chelate, free metal and free ligand, respectively. The pK_M of GdDTPA (22.5) is much higher than the pK_M of CaDTPA (10.7) and MgDTPA (9.3) (Dojindo, 2019). Thus, the binding competition of Ca^{2+} and Mg^{2+} in the hemolymph or seawater should be negligible. Indeed, in a separate experiment, the T_{1w}-MR image intensity of the kidney epithelia was not increased by incubation in seawater containing 1 mM of GdDTPA for 24 h. However, the K_M of MnEDTA (14.0) is higher, but closer to the K_M of CaEDTA (11.0) and MgEDTA (8.7) (Dojindo, 2019). It may be the case that MnEDTA releases free Mn^{2+} ion due to binding competition (Seo et al., 2013). In order to test the stability of MnEDTA, mussels were incubated in seawater containing 10 μM of MnEDTA for 1 h. There was no R_1 increase in the kidney due to the MnEDTA incubation, but R_1 was increased by the additional incubation with Mn^{2+} (P <0.05) (Fig. 7B). Therefore, MnEDTA is stable even at the concentration of 10 μM. It is also true that MnEDTA does not suffer Mn^{2+} uptake and concentration in the kidney.

DISCUSSION

Distribution of injected MR tracers

Tracer injection studies on the kidney started at the end of the 19th century, and the accumulation of indigo sulfonate (0.34 Da) was reported in the kidney of bivalves (Martin, 1983). Then, PAH (0.19 Da), PSP (0.35 Da) and inulin (5.5 kDa) appeared in the urine of *Haliotis rufescens* (Harrison, 1962). However, little knowledge was obtained due to the difficulty in obtaining consecutive samples of urine and blood from healthy, unrestrained bivalves (Martin, 1983). In this study, the concentration of MR tracers was estimated by employing the R_1 value, which precluded the need to insert a catheter in the mussel and the need to extract hemolymph or urine from the mussel. Except for the injection of MR tracers (5% of the volume of the hemolymph), the circulation of the hemolymph was not impeded. Therefore, this MRI technique is advantageous, compared with conventional invasive techniques. In regard to the results, we conclude that smaller MR tracers (Mn^{2+}, MnEDTA)

appeared in the urine in the kidney, while the larger MR tracers (CH3-DTPA-Gd and GdDTPA) stayed in the hemolymph.

In this study, we measured the whole body of the mussel by using 3D T_{1w}-MRI. In the beginning, the injected part of the visceral mass was depicted at a higher image intensity (Fig. 4A). Then, from 1 h to 3h after the injection of the MR tracers, the image intensity had reached to almost the same value in the visceral tissues, except for the kidney, digestive organs and the tip of the foot in some cases (Fig. 4F-I). Indeed, the R_1 values presented the same level for 3 h (P >0.05) (Fig. 5). Therefore, MR tracers were distributed fairly uniformly in the whole body, and were also stable in a time range of 1-3 h after the injection. We estimated the volume of the hemolymph (2.0 mL) using CH3-DTPA-Gd (Fig. 7). From the length of the shell, the wet weight of the mussel without the shell was estimated as 3.93 g (Hosomi, 1985), and the percentage of the hemolymph volume was estimated as 51% of the wet weight. This value is in good agreement with the previously reported values, 50.8 ± 7.6 % (mean and s.d.), of *M. californianus* measured by inulin (Martin et al., 1958). Thus, CH3-DTPA-Gd might be distributed in the same space as the inulin.

Molecular size dependency for filtration at the atrial wall

CH3-DTPA-Gd (2.1 kDa) and GdDTPA (0.55 kDa) were not accumulated in the urine of the kidney, but Mn^{2+} (0.055 kDa) and MnEDTA (0.35 kDa) were accumulated in that urine. Since there can be uptake of Mn^{2+} from the seawater, epithelial cells (probably in the digestive organ or gills) can transport Mn^{2+} (Fig. 1). Therefore, Mn^{2+} was filtrated at the atrial wall and it also might be secreted from the renal epithelial cells. As mentioned in the Introduction, Ca^{2+}, Mn^{2+} and Gd^{3+} share a close chemical similarity. Therefore, Mn^{2+} could be transported by the Ca^{2+} channel and Gd^{3+} could inhibit Ca^{2+}-dependent processes. If kidney epithelial cells uptake and secrete Mn^{2+}, there should be Gd^{3+} uptake in the epithelial cells, which may inhibit the epithelial functions. Indeed, Gd^{3+} was accumulated in the kidney epithelia (Fig. 4K), but was not concentrated in the urine (Fig. 6B). These results support that Gd^{3+} inhibits the epithelial functions. On the other hand, there was no uptake of MnEDTA and GdDTPA from the seawater in the kidney. Therefore, epithelial cells, not only in the

digestive organ but also in the kidney, could not transport MnEDTA and GdDTPA. This concept is supported by the lower MnEDTA concentration in the urine, compared with Mn^{2+} (Fig. 6B). Thus, MnEDTA must be filtered at the atrial wall, but GdDTPA was not. These results are in good agreement with the results of previous reports: indigo sulfonate (0.34 kDa) appeared in the urine of the kidney of bivalves, such as *Anodonta, Cardium, Tellina* etc (Martin, 1983), and injected PAH (0.19 kDa) and PSP (0.35 kDa) appeared in the urine of *Haliotis rufescens* (Harrison, 1962). Therefore, molecules smaller than 0.35 kDa can be filtered by the atrial wall. Harrison (1962) reported that concentration of urinary inulin was the same as the plasma in a wide range of the inulin concentration. This is not the case for GdDTPA or CH3-DTPA-Gd. The R_1 of the urine in the kidney remained the same as the R_1 in the control seawater (Fig. 6A). It is also true that MnEDTA in the urine is higher than that in the hemolymph (Fig. 6B). Therefore, it is not likely that inulin (5.5 kDa) is filtered by the atrial wall in *Mytilus*. Alternatively, *Haliotis rufescens* could filtrate larger molecules, and it is afraid that Harrison's methods (1962) might have lacked sufficient resolution or his experiments were prone to fluid contamination. We concluded that the molecular weight cut-off (MWCO) for filtration by the atrial wall of *Mytilus* is around 0.5 kDa, which is almost 1/100 (Gayton and Hall, 2006), of the MWCO for filtration by the glomerulus of the kidney in vertebrates, such as humans. The low MWCO may promote the maintenance of metabolites and osmolytes in the hemolymph, and save energy to reabsorb useful substances, such as glucose as reported for *Achatina fulica* (Martin et al., 1965). In the vertebrate, it is considered that a protein named nephrin controls the MWCO for filtration by the glomerulus (Kestilä et al., 1998), which forms the slit diaphragm. We are not sure nephrin can cover the wide range of the MWCO. Indeed, the MWCO at around 0.5 kDa is somehow similar to that controlled by the tight junction (Nitta et al., 2003). Therefore, in a future study, we plan to investigate the molecular-barrier mechanism in the atrial wall of *Mytilus* in which nephrin and claudin might be involved, and determine the protein responsible for the low MWCO.

In summary, we (1) injected 5 MR tracers in *M. galloprovincialis*, and detected the accumulation of the MR tracers in the urine of the kidney by MRI, and (2) MR tracers smaller than 0.35 kDa appeared in the kidney, but MR tracers larger than 0.5 kDa did not. Thus, the

MWCO is around 0.5 kDa, which is almost 1/100 of that for vertebrate animals, suggesting a reduction in efforts to reabsorb metabolites and osmolytes from the urine.

List of abbreviations

θ	flip angle
CH3-DTPA-Gd	oligomer-based contrast agent
GdDTPA	gadolinium-diethylenetriamine pentaacetic acid
K	relaxivity value of MR tracers
pK_M	Stability constant of metal complex
MnEDTA	manganese-ethylenediaminetetraacetic acid
MR	magnetic resonance
MRI	magnetic resonance imaging
MWCO	molecular weight cut-off
PAH	*p*-amino hippuric acid
PSP	phenolsuphonphthalein
R_1	longitudinal relaxation rate ($1/T_1$)
T_1	longitudinal relaxation time
T_{1w}-MRI	T_1-weighted gradient-echo magnetic resonance imaging
T_E	echo-time
T_R	relaxation delay

Acknowledgements

The authors would like to offer their sincere thanks to Dr. A. Kinjo-Kakumura and Prof. K. Inoue (AORI, UT) for providing the mussels. We would also like to express our thanks to Dr. D. Gross, Dr. V. Lehman and Dr. T. Oerther (Bruker Biospin), as well as Ms. Y. Imaizumi-Ohashi, Ms. M. Yokoi-Hayakawa and Ms. Kazuyo Mashiyama (DSUM) for their technical assistance. We must also thank Prof. S. Kojima (AORI, UT) for his helpful suggestions and encouragement to E.S.

Competing interests

The authors hereby declare there are no competing financial interests associated with this study.

Author contributions

H.W. and Y.S. conceived and designed the experiments; E.S. and H.W. performed the experiments; E.S. and Y.S. analyzed the data; and H.W. and Y.S. wrote the paper. All of the authors approved the final version of the manuscript.

Funding

Parts of this study were supported by grants from the JSPS KAKENHI (JP24659102 and JP15K08185 to Y.S.).

References

Andrews, E. B. and Jennings, K. H. (1993). The anatomical and ultrastructural basis of primary urine formation in bivalve molluscs. *J. Moll. Stud.* **59**, 223-257.

Bayne, B. L. (1976). *Marine mussels: their ecology and physiology.* 506pp. Cambridge: Cambridge University Press.

Boron, W. F. and Boulpaep, E. L. (2004). *Medical Physiology.* 1344pp. London: Saunders.

Brand, A. R. (1972). The mechanism of blood circulation in *Anodonta anatina* (L.) (Bivalvia, Unionidae). *J. Exp. Biol.* **56**, 361-379.

Burton, R. F. (1983). Ionic regulation and water balance. Chapter 6 In *Mollusca, Vol. 5*, (ed. A. S. M. Saleuddin and K. M. Wilbur), pp. 291-352. New York and London, Academic Press.

Dojindo (2019). Stability constants. Dojindo Molecular Technologies Inc, Kumamoto, Japan. data from: https://www.dojindo.eu.com/Images/Product%20Photo/Chelate_Table_of_ Stability_ Constants.pdf

Guyton, A. C. and Hall, J. E. (2006). *Textbook of Medical Physiology*, 11th edn. pp. 1116. Philadelphia: Elsevier Saunders.

Harrison, F. M. (1962). Some excretory processes in the abalone, *Haliotis rufescens*. *J. Exp. Biol.* **39**, 179-192.

Hosomi, A. (1985) On several fundamental allometries of the mussel *Mytilus galloprovincialis. Venus (Jap J Malacol)* **44**, 172-182.

Hoyaux, J., Gilles, R. and Jeuniaux, C. (1976). Osmoregulation in molluscs of the intertidal zone. *Comp. Biol. Physiol. A* **53**, 361-365.

Kestilä, M., Lenkkeri, U., Männikkö, M., Lamerdin, J., McCready, P., Putaala, H., Ruotsalainen, V., Morita, T., Nissinen, M., Herva, R., Kashtan, C. E., Peltonen, L., Holmberg, C., Olsen, A. and Tryggvason, K. (1998). Positionally cloned gene for a novel glomerular protein-nephrin-is mutated in congenital nephrotic syndrome. *Mol. Cell.* **1**, 575-582.

Krijgsman, B. J. and Divaris, G. A. (1955). Contractile and pacemaker mechanism of the heart of molluscs. *Biol. Rev.* **30**, 1-39.

Lin, Y. J. and Koretsky, A. P. (1997). Manganese ion enhances T_1-weighted MRI during brain activation: an approach to direct imaging of brain function. *Magn. Reson. Med.* **38**, 378-388.

Martin, A. W. (1983). Excretion. Chapter 7 In *Mollusca, Vol. 5*, (ed. A. S. M. Saleuddin and K. M. Wilbur), pp. 353-407. New York and London, Academic Press.

Martin, A. W. and Harrison, F. M. (1966). Excretion. Chapter 11 In *Physiology of Mollusca, Vol. II*, (ed. K. M. Wilbur and C. W. Yonge), pp. 353-386. New York and London, Academic Press.

Martin, A. W., Harrison, F. M., Huston, M. J. and Stewart, D. M. (1958). The blood volumes of some representative molluscs. *J. Exp. Biol.* **35**, 260-279.

Nitta, T., Hata, M., Gotoh, S., Seo, Y., Sasaki, H., Hashimoto N., Furuse, M. and Tsukita, S. (2003). Size-selective loosening of the blood-brain barrier in claudn-5-deficient mice. *J. Cell Biol.* **161**, 653-660.

Picken, L. E. R. (1937). The Mechanism of Urine Formation in Invertebrates. *J. Exp. Biol.* **14**, 20-34.

Pirie, B. J. S and George, S. G. (1979). Ultrastructure of the heart and excretory system of *Mytilus edulis* (L.). *J. Mar. Biol. Assoc. UK*. **59**, 819-829.

Ramsay, J. A. (1952). *A Physiological approach to the lower animals.* 149pp. Cambridge: Cambridge University Press.

Rogosnitzky, M. and Branch, S. (2016). Gadolinium-based contrast agent toxicity: a review of known and proposed mechanism. *Biometals.* **29**, 365-376.

Seo, E., Ohishi, K., Maruyama, T., Imaizumi-Ohashi, Y., Murakami, M. and Seo, Y. (2014a). Testing the constant-volume hypothesis by magnetic resonance imaging of the mussel heart in the *Mytilus galloprovincialis*. *J. Exp. Biol.* **217**, 964-973.

Seo, E., Ohishi, K., Maruyama, T., Imaizumi-Ohashi, Y., Murakami, M. and Seo, Y. (2014b). Magnetic resonance imaging analysis of water flow in the mantle cavity of live *Mytilus galloprovincialis. J. Exp. Biol.* **217**, 2277-2287.

Seo, E., Sazi, T., Togawa, M., Nagata, O., Murakami, M., Koima, S. and Seo, Y. (2016). A portable infrared photoplethysmograph: Heartbeat of *Mytilus galloprovincialis* analyzed by MRI and application to *Bathymodiolus septemdierum. Biol. Open.* **5**, 1752-1757.

Seo, Y., Satoh, K., Morita, H., Takamata, A., Watanabe, K., Ogino, T. and Murakami. M. (2013). Mn-citrate and Mn-HIDA: Intermediate-affinity chelates for manganese-enhanced MRI. *Contrast Media Mol. Imaging* **8**, 140-146.

Wakashin, H., Seo, E. and Seo, Y. (2018). Accumulation and excretion of manganese ion in the kidney of the *Mytilus galloprovincialis. J. Exp. Biol.* **221**: jeb.185439. doi: 10.1242/jeb.185439.

Yang, H., Wang, T., Li, J., Gu, L. and Zheng X. (2006). Decreasing expression of a_{1C} calcium L-type channel subunit mRNA in rat ventricular myocytes upon manganese exposure. *J. Biochem. Mol. Toxcol.* **20**, 159-166.

Figures

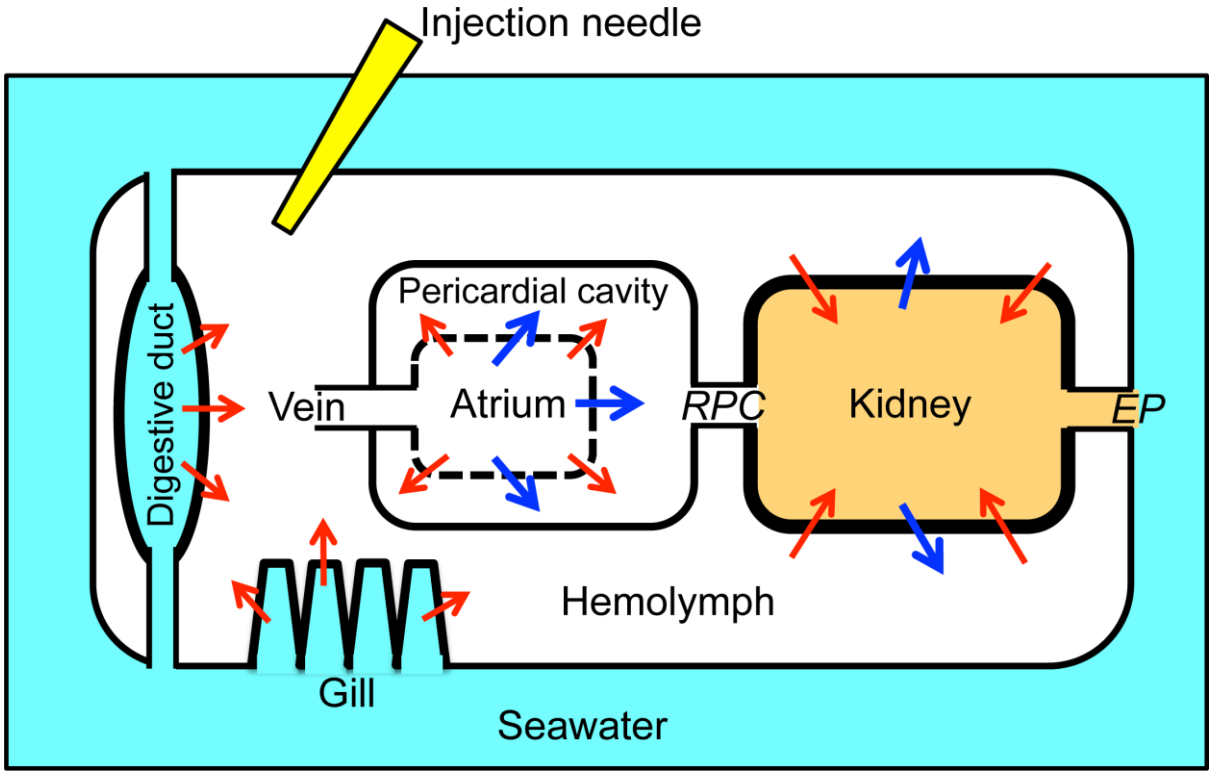

Fig. 1. Diagram of the excretion system of *M. galloprovincialis* incubated in Mn^{2+} containing seawater. When mussels are incubated in Mn^{2+} containing seawater, epithelial cells of digestive organs and gills uptake Mn^{2+} into the hemolymph. The Mn^{2+} is filtered by the atrial wall into the pericardial cavity. Then, water is reabsorbed and Mn^{2+} is secreted by the kidney epithelia. As a result, Mn^{2+} is accumulated in the kidney (Wakashin et al., 2018). Filtration and reabsorption of hemolymph are shown by blue arrows. Filtration and transport of Mn^{2+} are shown by red arrows. Labelled features: (*EP*) excretory pore, (*RPC*) renopericardial canal. The position of injected needle is also shown. It is expected that the transport of Mn^{2+} in epithelial cells (kidney, digestive organ and gill) and water in kidney epithelium is inhibited by Gd^{3+}.

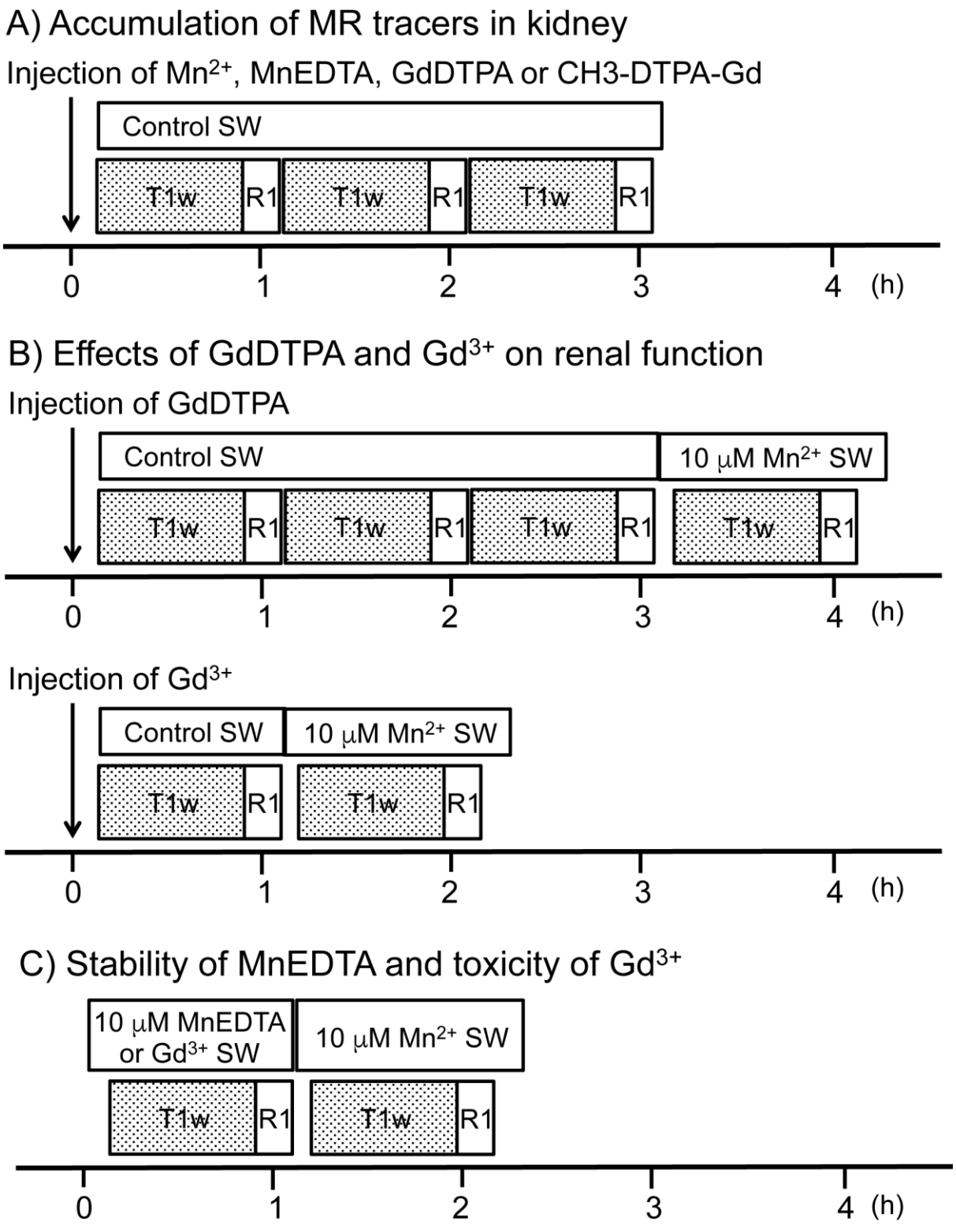

Fig. 2. Protocols of the MR tracer experiments. (A) Accumulation of injected MR tracers in the kidney. (B) The effects of the injected GdDTPA and Gd^{3+} on renal function. (C) Incubation study to test the stability of the MnEDTA and the toxicity of Gd^{3+}. Labelled features: (Control SW) incubated in control seawater, (10 μM Mn^{2+} SW) incubated in seawater containing 10 μM of $MnCl_2$, (T1w) measurement of 3D T_{1w}-MR image, (R1) measurement of R_1. The long arrows indicate the injection of the MR tracers. Details are presented in the text.

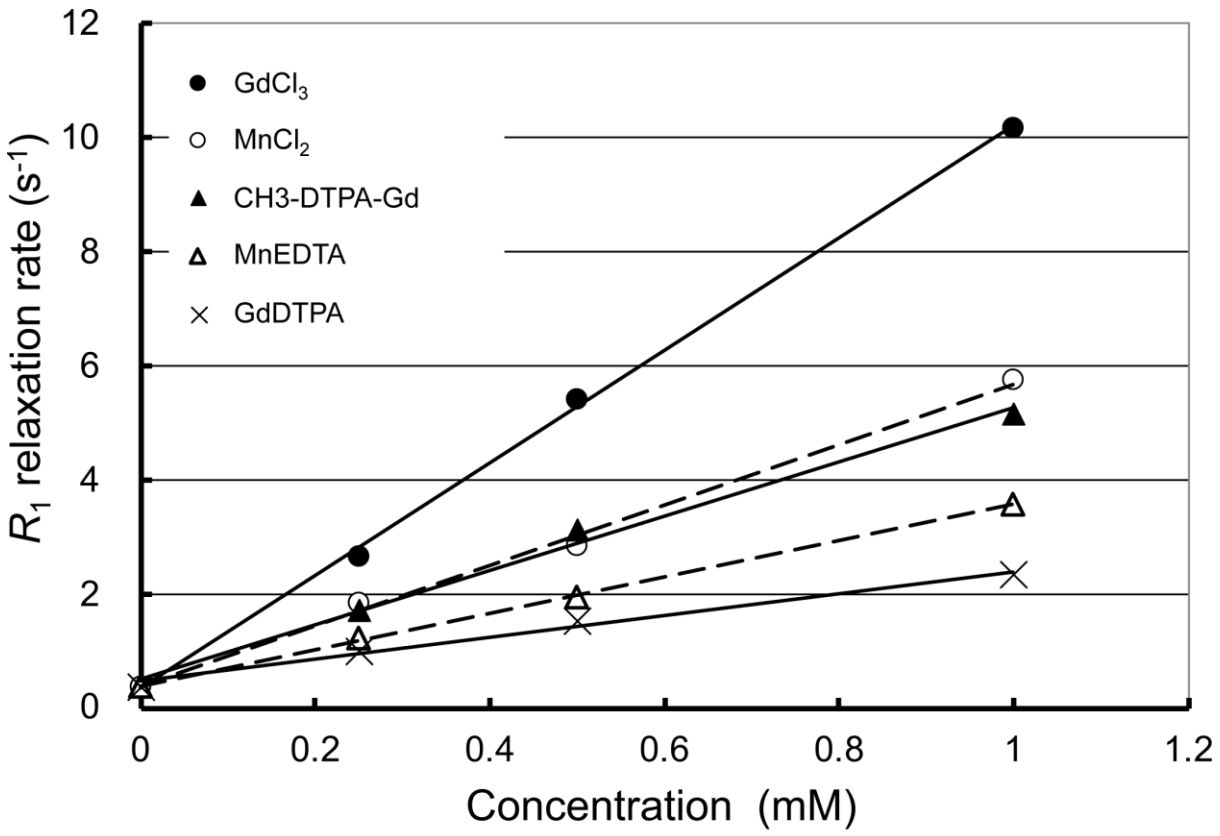

MR tracer	Relaxivity ($(s \cdot mM)^{-1}$)	±95% confidence interval
$GdCl_3$	9.87	0.87
$MnCl_2$	5.30	0.99
CH3-DTPA-Gd	4.76	1.17
MnEDTA	3.19	0.16
GdDTPA	1.93	0.64

Fig. 3. Concentration dependence of the R_1 relaxation rate of MR tracer containing 36‰ NaCl solution at 20°C. The lines shown represent a linear regression between R_1 and the concentration of the MR tracers. The relaxivity of the MR tracers (coefficient and ± 95% confidence interval) were calculated from the slope, and are summarized in the table.

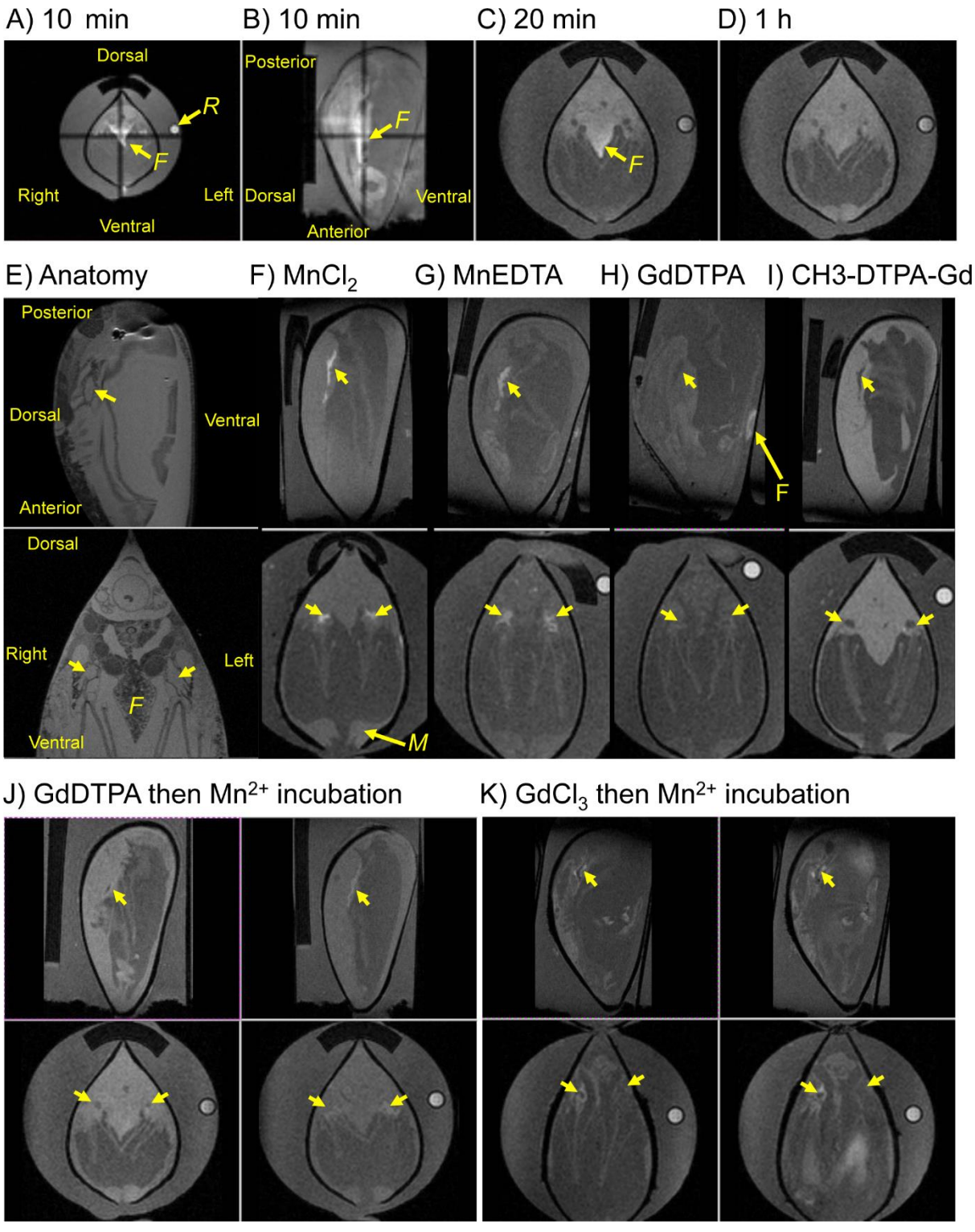

Fig. 4. Distribution of injected MR tracers in *M. galloprovincialis* imaged by T_{1w}-MRI.

(A-D) Time dependent changes after injection of 0.1 mL of 2 mM GdDTPA. (A) Transverse and (B) sagittal images 10 min after injection. (C) 20 min and (D) 1 h after injection.

(E-I) Two hours after the injection of the MR tracers. Pairs of longitudinal slices at the kidney and a transverse slice 2 mm posterior to the atrioventricular valve are shown. (E) Anatomical images obtained by paraformaldehyde fixed mussel. (F) 0.1 mL of 1 mM $MnCl_2$. (G) 0.1 mL of 1 mM MnEDTA. (H) 0.1 mL of 1 mM GdDTPA. (I) 0.1 mL of 1 mM CH3-DTPA-Gd.

(J-K) One hour after the injection of the MR tracers followed by 1 h additional incubation in seawater containing 10 μM of $MnCl_2$. (J) Left panels: injection of 0.1 mL of 2 mM GdDTPA. Right panels: additional incubation in Mn^{2+}. (K) Left panels: injection of 0.1 mL of 1 mM $GdCl_3$. Right panels: additional incubation in Mn^{2+}. Labelled features: (*F*) foot, (*M*) mantle, (*R*) Reference capillary containing 0.5 mM of $MnCl_2$. The short arrows indicate the kidney.

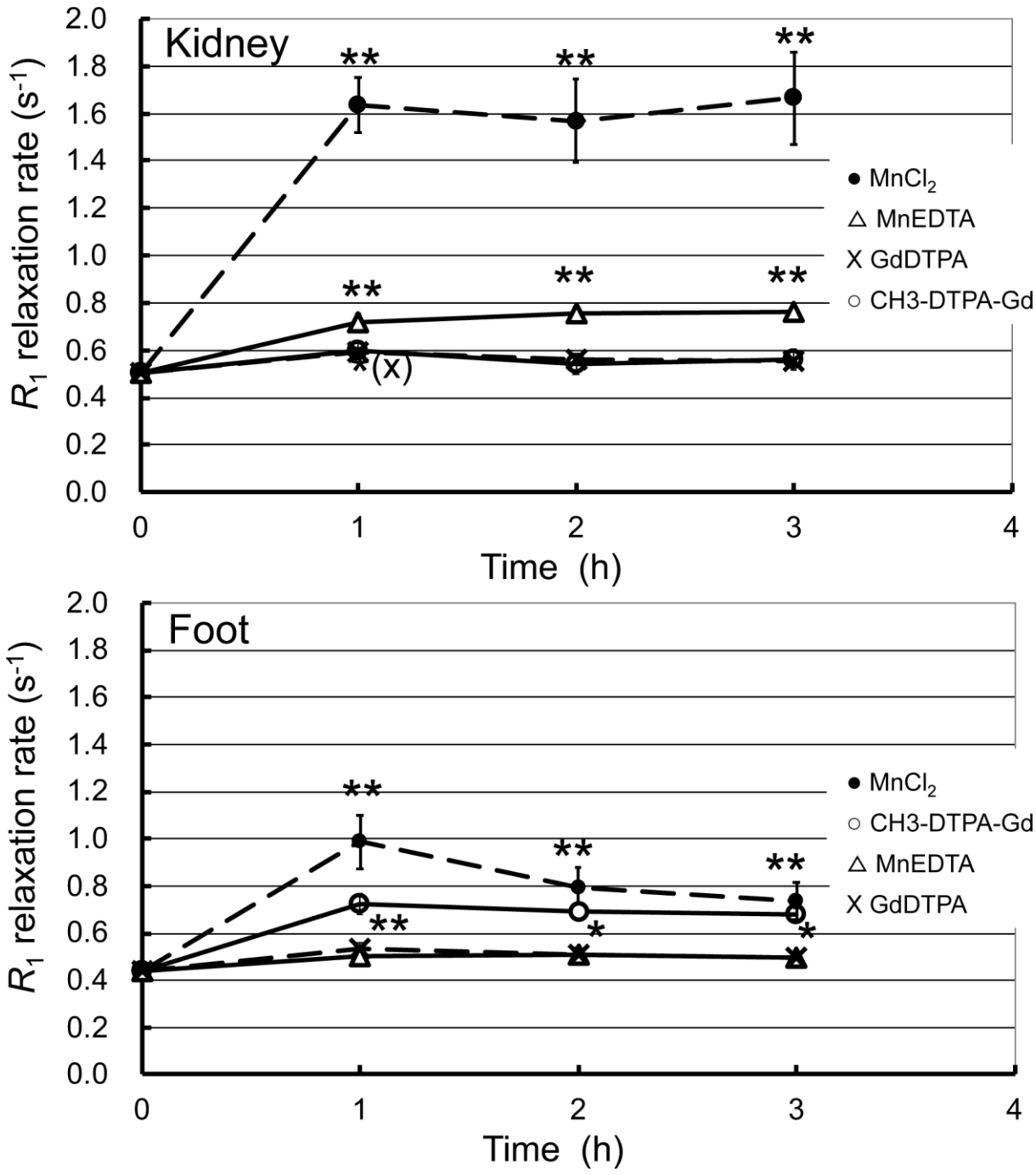

Fig. 5. Changes in the R_1 relaxation rate of the kidney and foot after the injection of MR tracers. Means (± s.e.m.) of the R_1 of the kidneys and feet at 1, 2 and 3 h after injection of the MR tracers (1 mM x 0.1 mL). The numbers of kidneys and feet studied were 10-14 and 5-7, respectively. Significant statistical differences compared with R_1 in the control seawater (0 h, 56 kidneys and 28 feet) were shown by * (P <0.05) and ** (P <0.01). There were no significant differences shown in R_1 from 1 h to 3 h for any of the MR tracers (P >0.05).

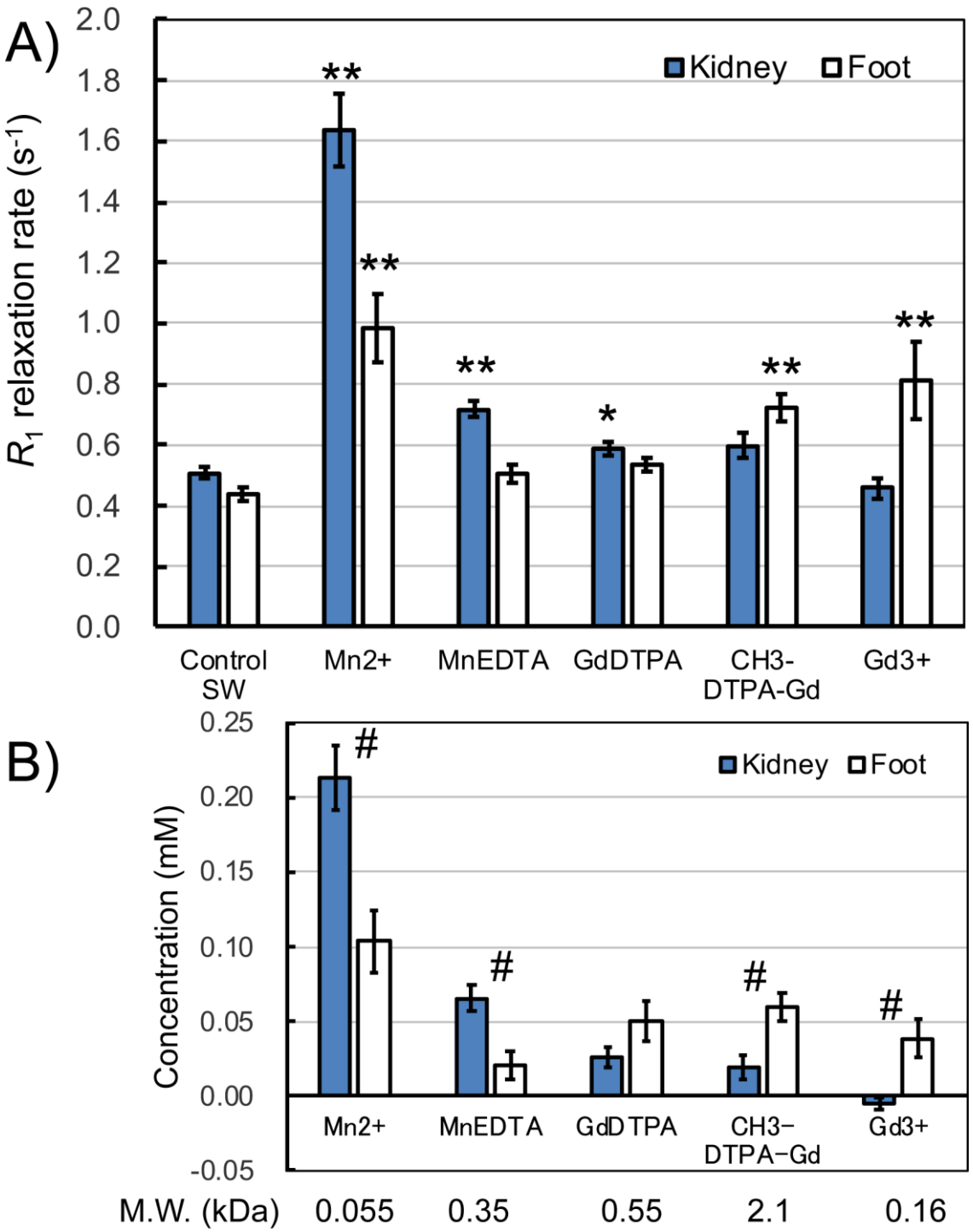

Fig. 6. R_1 relaxation rate and MR tracers concentration in the kidney and foot after the injection of MR tracers. (A) Means (± s.e.m.) of R_1 of the kidneys and feet at 1 h after injection of the MR tracers (1 mM x 0.1 mL). The number of kidneys and feet were 10-14 and 5-7, respectively. Significant statistical differences compared with R_1 in the control seawater (Control SW, 56 kidneys and 28 feet) were shown by * (P <0.05) and ** (P <0.01). (B) Means (± s.e.m.) of the concentration of the MR tracers of the kidneys and feet calculated from the increase in R_1 and the relaxivity of the MR tracers (Fig. 1). Significant statistical differences between the kidney and foot for each of the MR tracers were shown by # (P <0.01).

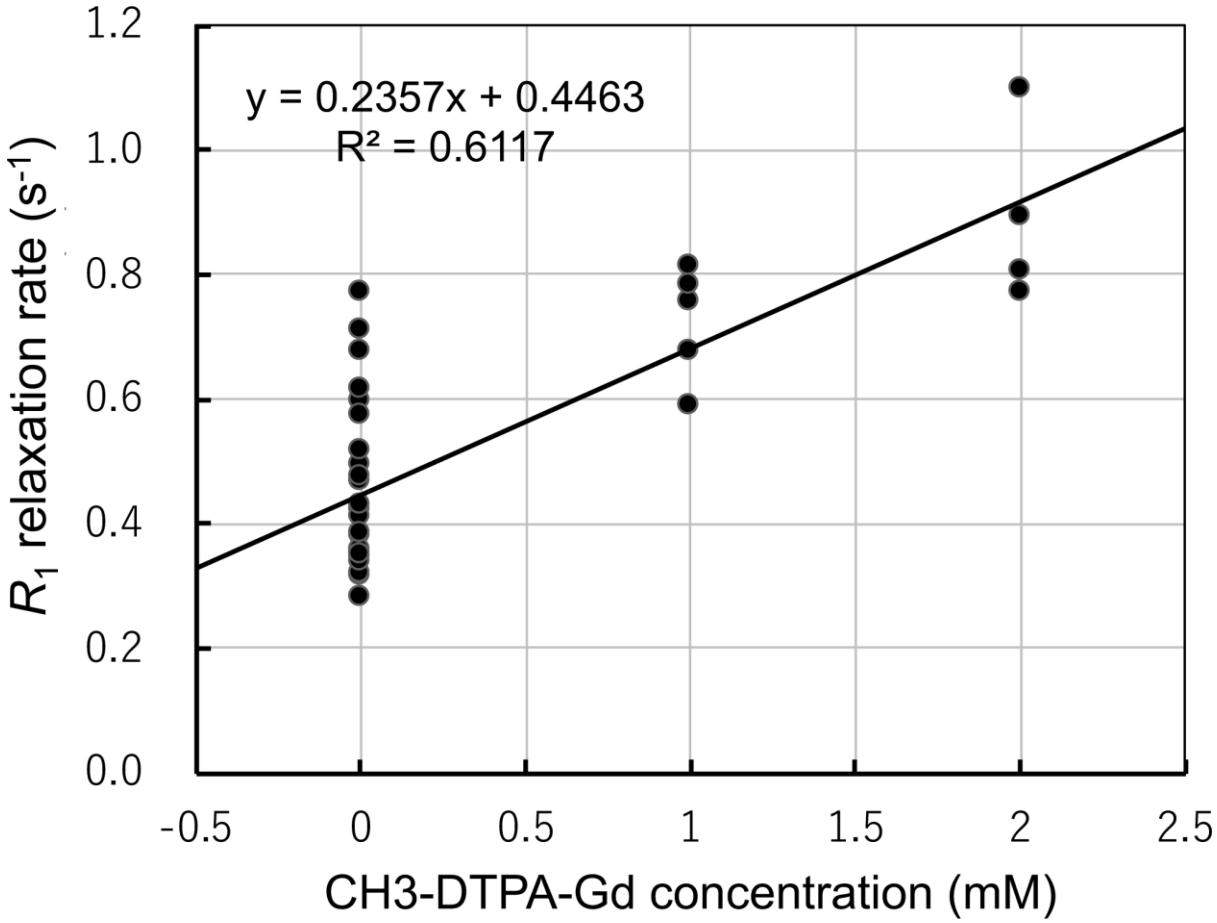

Fig. 7. Concentration dependence of the R_1 relaxation rate of the foot 1 h after the injection of CH3-DTPA-Gd. The bold line represents a linear regression between R_1 and the CH3-DTPA-Gd concentration. The slope of the regression line is 0.236 $s^{-1}\cdot mM^{-1}$, and R is the correlation coefficient of the regression.

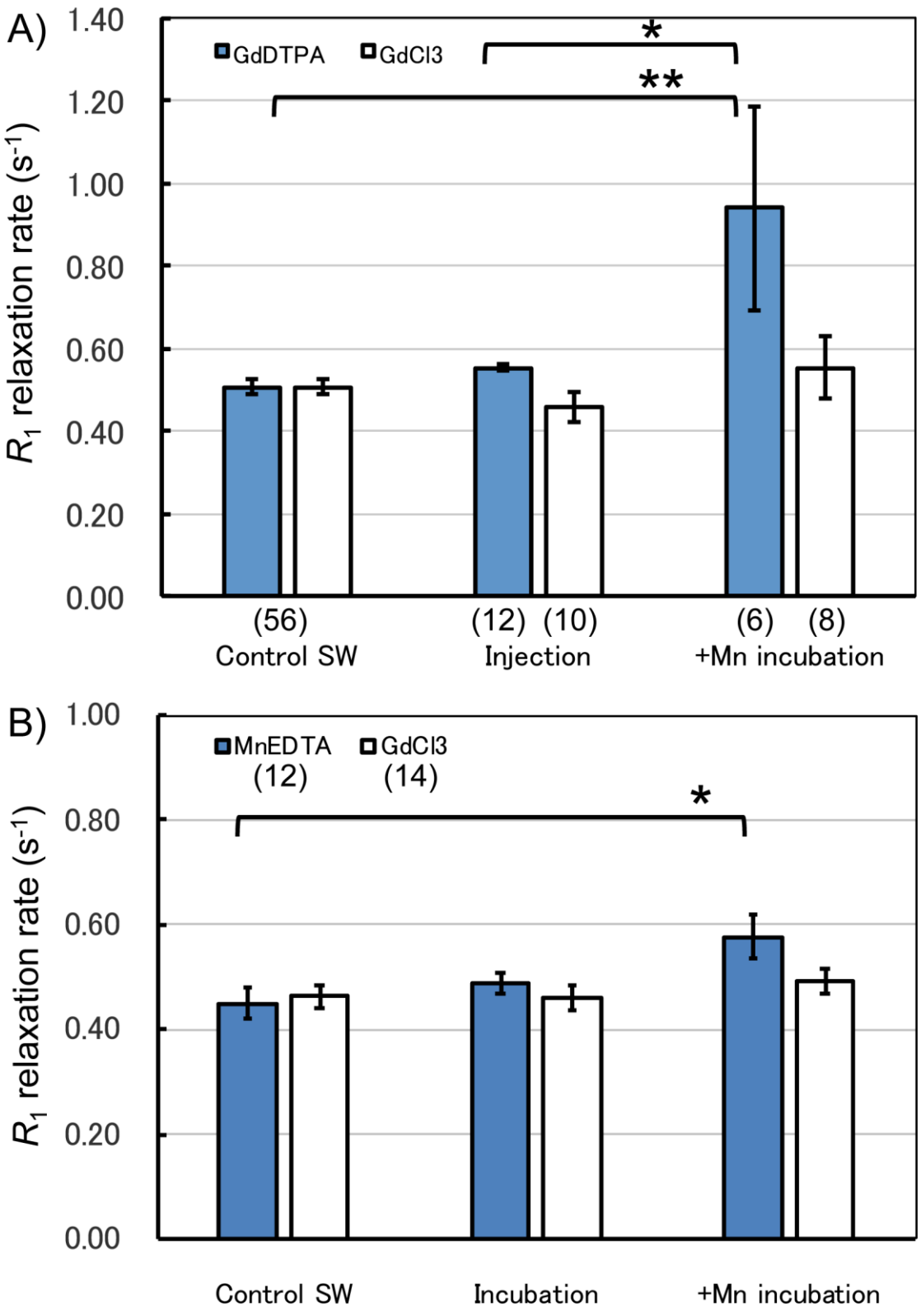

Fig. 8. Uptake of GdDTPA, MnEDTA and $GdCl_3$ in the kidney of *Mytilus galloprovincialis*. (A) Means (± s.e.m.) of the R_1 of the kidneys in the control seawater (Control SW), 3 h or 1 h after the injection of 1 mM GdDTPA or $GdCl_3$, respectively (Injection), and additional incubation in seawater containing 10 μM of $MnCl_2$ for 1 h (+Mn incubation). (B) Means (± s.e.m.) of the R_1 of the kidneys before (Control SW) and after incubation in seawater containing 10 μM of MnEDTA or $GdCl_3$ for 1 h (Incubation), and additional incubation in seawater containing 10 μM of $MnCl_2$ for 1 h (+Mn incubation). Numbers in parenthesis are the number of kidneys. Significant statistical differences were shown by * (P <0.05) and ** (P <0.01).